Live cell micropatterning reveals the dynamics of signaling complexes at the plasma membrane

Sara Löchte,* Sharon Waichman,* Oliver Beutel, Changjiang You, and Jacob Piehler

Department of Biology, University of Osnabrück, 49076 Osnabrück, Germany

Interactions of proteins in the plasma membrane are notoriously challenging to study under physiological conditions. We report in this paper a generic approach for spatial organization of plasma membrane proteins into micropatterns as a tool for visualizing and quantifying interactions with extracellular, intracellular, and transmembrane proteins in live cells. Based on a protein-repellent poly(ethylene glycol) polymer brush, micropatterned surface functionalization with the HaloTag ligand for capturing HaloTag fusion proteins and RGD peptides promoting cell adhesion was devised. Efficient micropatterning of the type I interferon (IFN) receptor subunit IFNAR2 fused to the HaloTag was achieved, and highly specific IFN binding to the receptor was detected. The dynamics of this interaction could be quantified on the single molecule level, and IFN-induced receptor dimerization in micropatterns could be monitored. Assembly of active signaling complexes was confirmed by immunostaining of phosphorylated Janus family kinases, and the interaction dynamics of cytosolic effector proteins recruited to the receptor complex were unambiguously quantified by fluorescence recovery after photobleaching.

Introduction

Transport and communication across the plasma membrane are mediated by large, dynamic multiprotein complexes. The molecular interactions controlling assembly and dynamics of these complexes are notoriously difficult to study as a result of their low density and often rather homogeneous distribution within the plasma membrane. Sophisticated protein–protein interaction networks have been assembled over the past decades by combining genetic and biochemical assays, including yeast two-hybrid screens, coimmunoprecipitation, and pull-down experiments (Barrios-Rodiles et al., 2005; Suter et al., 2008; Vermeulen et al., 2008), yet robust methods for validation and quantification of interactions involving membrane proteins under physiological conditions are still missing. Current techniques for quantitative protein interaction analysis in live cells, such as Förster resonance energy transfer (Day and Davidson, 2012; Padilla-Parra and Tramier, 2012; Sun et al., 2012) or fluorescence cross-correlation spectroscopy (Kim et al., 2007; Bleicken et al., 2011; Ries and Schwille, 2012) are highly demanding and often fail in case of low affinity, transient interactions, or large multiprotein complexes in the context of membranes. For these reasons, quantitative analysis of interactions within transmembrane signaling complexes remains particularly challenging.

Here, we aimed to establish a generic method exploring protein interactions involved in the formation of signaling complexes at the plasma membrane. To this end, we developed a surface architecture for spatial organization of transmembrane receptors within the plasma membrane of live cells. Capturing of transmembrane receptors in living cells by patterning ligands or antibodies on solid support has been pioneered and was applied very successfully for studying spatial regulation of signaling processes (Torres et al., 2008a,b; Salaita et al., 2010; Xu et al., 2011; Gandor et al., 2013) and the assembly of signaling complexes (Schwarzenbacher et al., 2008; Arrabito et al., 2013; Sunzenauer et al., 2013; Lanzerstorfer et al., 2014) in a systematic and quantitative manner. Here, we have expanded this concept toward a generic methodology for quantitative interaction analysis with bait proteins micropatterned within the plasma membrane of living cells. To this end, target proteins were fused to the HaloTag, which covalently binds to a chlorohexane-functionalized ligand (HaloTag ligand [HTL]) in a highly specific

*S. Löchte and S. Waichman contributed equally to this paper.

Correspondence to Jacob Piehler: piehler@uos.de

Abbreviations used in this paper: HTL, HaloTag ligand; IFNAR, IFN receptor; JAK, Janus family kinase; MBP, maltose binding protein; PEG, poly(ethylene glycol); ROI, region of interest; STAT, signal transducer and activator of transcription; TIR, total internal reflection; TIRF, TIR fluorescence; TMD, transmembrane domain.

The Rockefeller University Press $30.00
J. Cell Biol. Vol. 207 No. 3 407–418
www.jcb.org/cgi/doi/10.1083/jcb.201406032

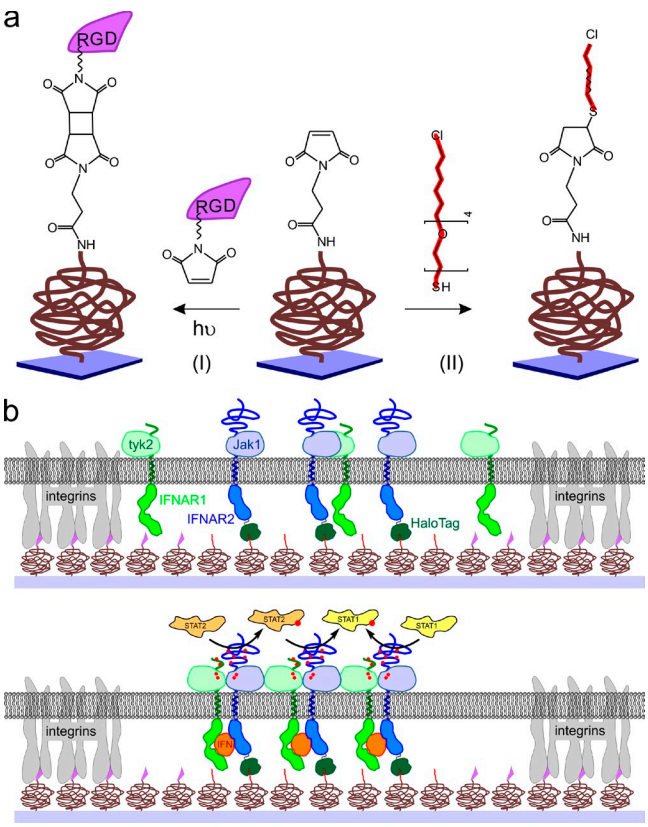

Figure 1. **Strategies for assembly of functional signaling complexes into micropatterns.** (a) Binary surface patterning by photochemical coupling of maleimido-RGD to a maleimide-functionalized PEG polymer brush (I) followed by reaction of the nonilluminated maleimide groups with a thiol-functionalized HTL (II). (b) Concept of spatial organization of IFN receptor signaling complexes in the plasma membrane of cells cultured on the surface of a micropatterned coverslide. (top) IFNAR2 fused to the HaloTag is captured into HTL-functionalized areas (HTL functionalities are depicted in red), whereas cell attachment via focal adhesions is mediated by RGD-functionalized areas (RGD functionalities are depicted in violet). (bottom) Upon addition of the IFN, functional complexes are formed by recruitment of IFNAR1 (green), leading to phosphorylation of the associated JAK kinases Jak1 and tyk2 as well as of tyrosine residues on the cytosolic domains of the receptor subunits. Thus, effector proteins such as STAT1 and STAT2 are locally recruited to the receptor.

manner (Los et al., 2008). For spatially resolved capturing of HaloTag fusion proteins in the plasma membrane of live cells, we implemented functional micropatterning on the basis of a biocompatible surface architecture with minimum nonspecific protein binding properties. Thus, interactions can be probed not only with proteins in the cytoplasm but also with exogenous proteins such as ligands binding to cell surface receptors, as required for the assembly of entire signaling complexes. For this purpose, a protein-repelling ultrathin poly(ethylene glycol) (PEG) polymer brush was used, which also inhibits cell adhesion on the surface. Highly orthogonal, binary patterning of an RGD peptide and HTL was developed for efficient attachment of cells and for capturing of the bait protein, respectively. To this end, we established photo–cross-linking of surface maleimide groups with a maleimide-functionalized compound in solution (Fig. 1 a).

We have here applied this approach to unravel the protein–protein interactions involved in the formation of the IFN signaling complex. The IFN receptor (IFNAR) is comprised of two subunits, IFNAR1 and IFNAR2 (Cohen et al., 1995; Uzé et al., 2007), which both independently interact with the ligand (Lamken et al., 2005; Li et al., 2008; Thomas et al., 2011), thus forming a ternary complex (Fig. 1 b). IFNs bind IFNAR2 with substantially higher binding affinity (lower nanomolar regimen) than IFNAR1 (micromolar regimen; Lamken et al., 2004; Jaks et al., 2007; Lavoie et al., 2011). IFN-mediated receptor dimerization leads to phosphorylation of the cytosolic Janus family kinases (JAKs) tyk2 and Jak1, which are noncovalently associated with IFNAR1 and IFNAR2, respectively (Prejean and Colamonici, 2000). Signal transducers and activators of transcription (STATs), STAT1 and STAT2, are recruited to the receptor and phosphorylated by tyk2 and/or Jak1 to form homodimers (pSTAT1/pSTAT1) and heterodimers (pSTAT1/pSTAT2), which translocate into the nucleus and regulate transcription. Recently, the USP18 (ubiquitin-specific protease 18) has been identified as a key regulator of IFN signaling, which was suggested to interact with IFNAR2 (Malakhova et al., 2006) and modulate receptor assembly (François-Newton et al., 2011). Although some of the protein–protein interactions involved in receptor assembly and effector recruitment have been characterized by pull-down experiments, these do not provide a mechanistic view of the spatiotemporal organization of the IFN transmembrane signaling complex. Open questions include a potential predimerization of IFNAR1 and IFNAR2, which has been suggested for other cytokine receptors (Remy et al., 1999; Kubatzky et al., 2001; Grötzinger, 2002; Pang and Zhou, 2012), the dynamics of JAK association with the receptor subunits (Haan et al., 2006), and the role of the determinants of STAT1 and STAT2 recruitment (Prejean and Colamonici, 2000) as well as the mechanism of USP18 negative feedback for IFN signaling (Francois-Newton et al., 2011, 2012). We demonstrate here how micropatterning of the receptor subunits within the plasma membrane of live cells provides versatile means to address these fundamental questions in cytokine receptor research.

Results

Binary functional patterning of maleimide-functionalized surfaces

To obtain high-contrast micropatterns of target proteins while restricting focal adhesion outside these zones, an efficient binary patterning technique was implemented. To this end, we exploited the photoactivation of maleimides by UV illumination (Yamada et al., 1968) for spatially resolved surface functionalization. We have previously used this approach for micropatterning by maleimide photodestruction (Waichman et al., 2011) and by photochemical coupling of hydrophobic tethers via vinyl ether groups (Waichman et al., 2013). Here, we established cross-linking of photoactivated maleimide groups on the surface with maleimide-functionalized ligands in solution for binary patterning (Fig. 1 a). Surface modification by photochemical maleimide cross-linking was quantitatively assessed by solid-phase detection using reflectance interference spectroscopy

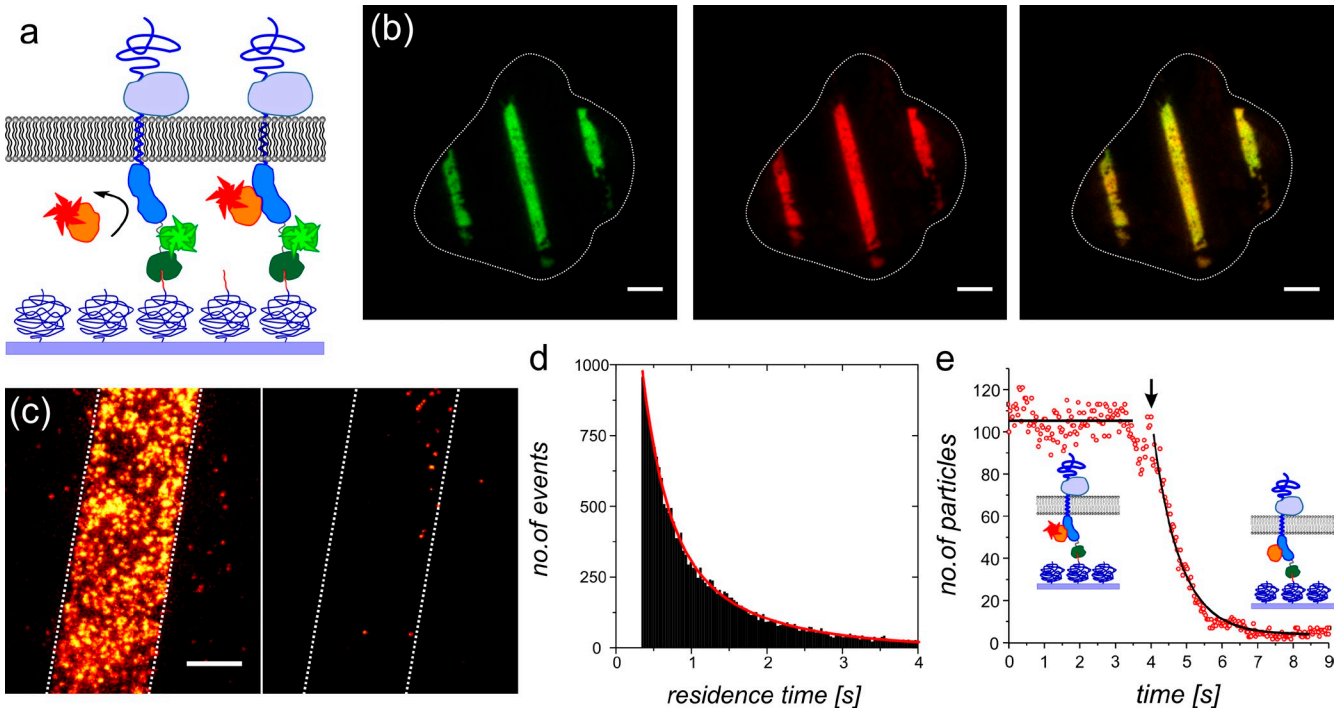

Figure 2. **Capturing of IFNAR2 into micropatterns.** (a) IFNAR2 (blue) fused to EGFP (green) and the HaloTag (dark green) was transiently transfected into HeLa cells and cultured on a micropatterned support. Ligand binding was probed by incubating 10 nM ^{AT655}IFNα2 (red–orange). (b) Fluorescence intensity within a single HeLa cell expressing HaloTag-EGFP-IFNAR2 (green channel) after incubation of ^{AT655}IFNα2 (red channel). The overlay of both channels is shown in the right image. Dotted lines indicate the boundaries of the cells. Bars, 10 µm. (c–e) Reversible ligand binding quantitatively probed by single-molecule imaging of the low-affinity mutant ^{DY647}IFNα2 M148A-NLYY. (c) Superimposition of 200 consecutive frames in the presence of 0.5 nM ^{DY647}IFNα2 M148A-NLYY before (left) and after (right) chasing with unlabeled IFNα2-α8tail-YNS. Dotted lines indicate the analyzed line pattern. Bar, 5 µm. (d) Dwell time distribution obtained from single-molecule localization experiments in micropatterns (20,870 binding events from the cell shown in c, representative for three cells analyzed). Only molecules localized for >10 consecutive frames (320 ms) were evaluated. (e) Displacement kinetics in micropatterns upon chasing with unlabeled IFNα2-α8tail-YNS (injection marked with an arrow) and fit of the curve (representative of three cells analyzed).

(Schmitt et al., 1997). For this purpose, biotin maleimide was reacted with maleimide-functionalized surfaces by UV irradiation, and binding of streptavidin was probed (Fig. S1). Rapid and highly efficient coupling of biotin maleimide was detected, which was not detectable without irradiation. These results confirmed efficient photochemical surface functionalization as well as negligible nonspecific binding to the PEG polymer brush. The same approach was used for photopatterning of maleimide-functionalized RGD for promoting cell adhesion on the protein-repelled PEG polymer brush followed by reaction of HTL-thiol with intact maleimide groups within the nonilluminated areas (compare Fig. 1 a). Upon micropatterned surface functionalization with HTL, high-contrast binding of the HaloTag fused to monomeric EGFP (HaloTag-EGFP) into HTL-functionalized regions was confirmed (Fig. S1).

Receptor micropatterning and IFN binding

For visualizing micropatterns of the IFNAR subunit IFNAR2 within cells, we fused IFNAR2 to both monomeric EGFP and the HaloTag (HaloTag-EGFP-IFNAR2), which was transiently expressed in HeLa cells under control of the cytomegalovirus promoter. HeLa cells—as all nucleated cells—express endogenous IFNAR1 and IFNAR2, yet at very low surface concentrations (~500 copies/cell). Thus, negligible background from the endogenous receptor is expected. HeLa cells transfected with HaloTag-EGFP-IFNAR2 were cultured on a coverslide functionalized with RGD and HTL in subcellular dimension (compare Fig. 2 a) and imaged at the surface-proximal cellular membrane by total internal reflection (TIR) fluorescence (TIRF) microscopy. Strikingly, successful reorganization of IFNAR2 in the plasma membrane of a transfected cell following the line structure of the photomask used for patterning was observed with high contrast (Fig. 2 b). Upon incubation of the ligand, IFNα2 site-specifically labeled with ATTO 655 (^{AT655}IFNα2) binding into the same zones occupied by IFNAR2 was observed. Staining of the entire micropatterned substrate with a purified HaloTag-EGFP fusion protein confirmed IFNα2 binding within HTL-functionalized areas (Fig. S2). In contrast, expression of IFNAR2 without a HaloTag resulted into homogeneous distribution of ^{AT655}IFNα2 on the entire cell surface (Fig. S2). Thus, not only efficient micropatterning of IFNAR2 was achieved but also the functionality of its extracellular ligand binding domain and its accessibility by IFN was preserved.

IFNα2 binds with an affinity of ~5 nM to IFNAR2, corresponding to a dissociation rate constant of ~0.02 s^{-1} (Piehler and Schreiber, 1999; Strunk et al., 2008). For probing the dynamics of this interaction in a quantitative manner, we used the IFNα2 mutant M148A in combination with the mutations N65A, L80A, Y85A, and Y89A (M148A-NLYY; Piehler et al., 2000b; Roisman et al., 2005), which binds IFNAR2 with ~50-fold

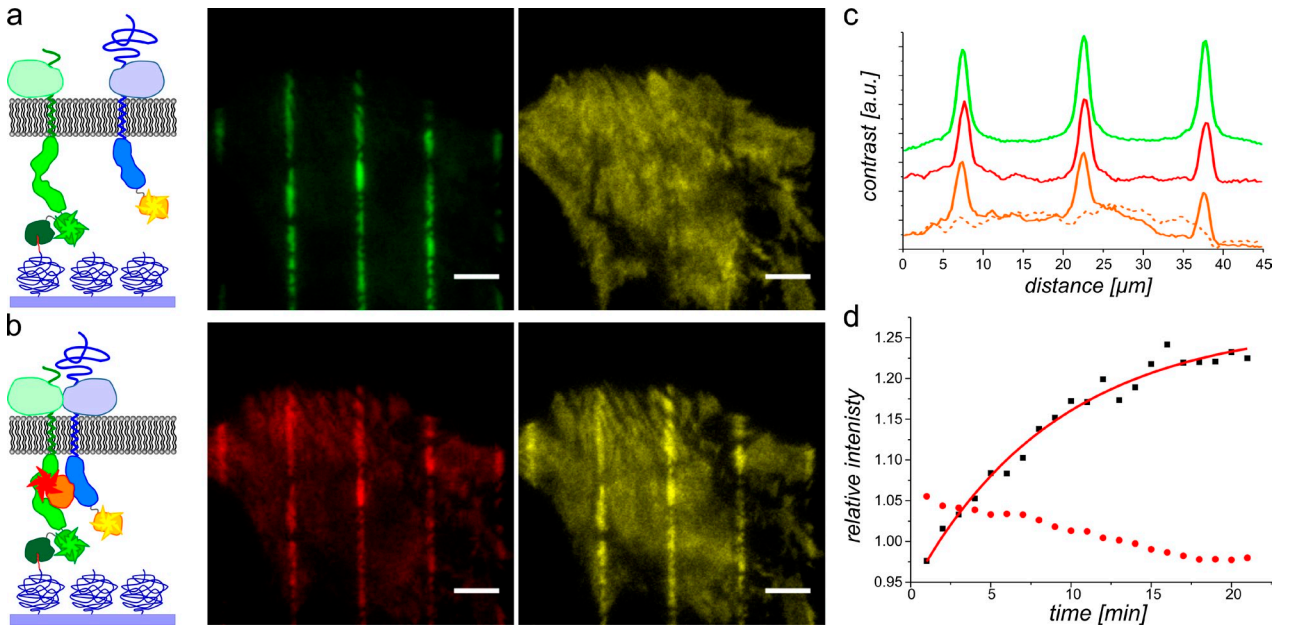

Figure 3. **Ternary complex assembly in micropatterns.** (a and b) HaloTag-EGFP-IFNAR1 (green channel) expressed in HeLa cells together with TagRFP-IFNAR2 (yellow channel) and cultured on a micropatterned support before (a) and 20 min after (b) addition of ^{AT655}IFNα2 (red channel). Bars, 10 µm. (c) Distribution IFNAR1 (green), IFNAR2 (orange), and IFNα2 (red) after formation of the ternary complex (representative of two cells analyzed). For comparison, the distribution of IFNAR2 before addition of IFNα2 (orange, dotted line) is shown. Integrated line profiles were scaled to similar amplitudes and overlaid at an arbitrary ordinate scale. a.u., arbitrary unit. (d) Time-resolved increase of the IFNAR2 concentration within (black squares) and decrease outside IFNAR1 micropatterns (red dots). Intensities normalized to the intensities outside the functionalized areas are plotted (representative of two cells analyzed).

increased dissociation rate constant, whereas binding to endogenous IFNAR1 is negligible (the binding properties of IFNα2 mutants are summarized in Table S1). Binding of IFNα2 M148A-NLYY labeled with DY-647 (^{DY647}IFNα2 M148A-NLYY) to micropatterned IFNAR2 was monitored by single-molecule imaging. Transient binding specifically within the micropatterns was observed as expected for this ligand (Video 1 and Fig. 2 c) and confirmed by single-molecule bleaching at elevated laser power (Arant and Ulbrich, 2014). No lateral diffusion was observed for ligands bound within the micropattern as expected for immobilized IFNAR2. Thus, the lifetime of the complex could be determined reliably by the analysis of the residence time of individual molecules within the pattern (Fig. 2 d). An exponential decay was observed, yielding a dissociation rate constant of 1.25 ± 0.23 s^{-1}, which is in very good agreement with the rate constant found for this interaction in vitro by ensemble and single-molecule imaging techniques (Waichman et al., 2011, 2013). Specific and reversible ligand binding to micropatterned IFNAR2 was furthermore confirmed by chasing with unlabeled IFNα2-α8tail-YNS (H57Y, E58N, and Q61S), which binds IFNAR with substantially higher affinity (Levin et al., 2011). Rapid displacement of ^{DY647}IFNα2 M148A-NLYY was observed as was very low residual binding (Video 2 and Fig. 2 e). The fluorescence decay within the pattern was fitted by a single exponential, yielding a dissociation rate constant of 1.15 ± 0.20 s^{-1} in good agreement with the single molecule data. These studies not only confirmed the high patterning efficiency and full functionality of micropatterned IFNAR2 but also the compatibility of this approach with quantitative binding assays by ensemble and single-molecule detection techniques.

Formation of the ternary signaling complex

In the next step, we explored the assembly of the ternary signaling complex induced by IFNα2, which can interact simultaneously with IFNAR1 and IFNAR2 via independent binding sites (Thomas et al., 2011). IFNAR1 binds IFNα2 with a K_d of 5 µM affinity, a binding affinity that is three orders of magnitude lower than the binding affinity toward IFNAR2 (Lamken et al., 2004). Owing to these very asymmetric binding affinities, IFNα2 interaction with IFNAR1 is believed only to occur after binding to the high-affinity subunit IFNAR2. However, predimerization of the receptor subunits in its absence has been suggested for several cytokine receptors including the IFNAR (Remy et al., 1999; Kubatzky et al., 2001; Grötzinger, 2002; Krause et al., 2002, 2013; Brown et al., 2005; Pang and Zhou, 2012).

Here, we used spatial redistribution with micropatterned receptors to unambiguously probe receptor dimerization in living cells. Control experiments revealed that micropatterning caused only minor changes in the membrane-proximal cytoskeleton (Fig. S3) and no changes in the diffusion properties of membrane proteins (Fig. S3). To explore assembly of the ternary IFN–receptor complex, HeLa cells were transiently transfected with IFNAR1 fused to the HaloTag and monomeric EGFP (HaloTag-EGFP-IFNAR1) and with IFNAR2 fused to TagRFP-T (TagRFP-IFNAR2). Upon culturing these cells on a micropatterned support, IFNAR1 was captured into micropatterns, whereas homogeneous distribution of IFNAR2 was observed (Fig. 3 a). After incubation of ^{AT655}IFNα2 for a few minutes, recruitment of IFNAR2 into the micropatterns was observed (Video 3 and Fig. 3 b). The excellent congruence of the

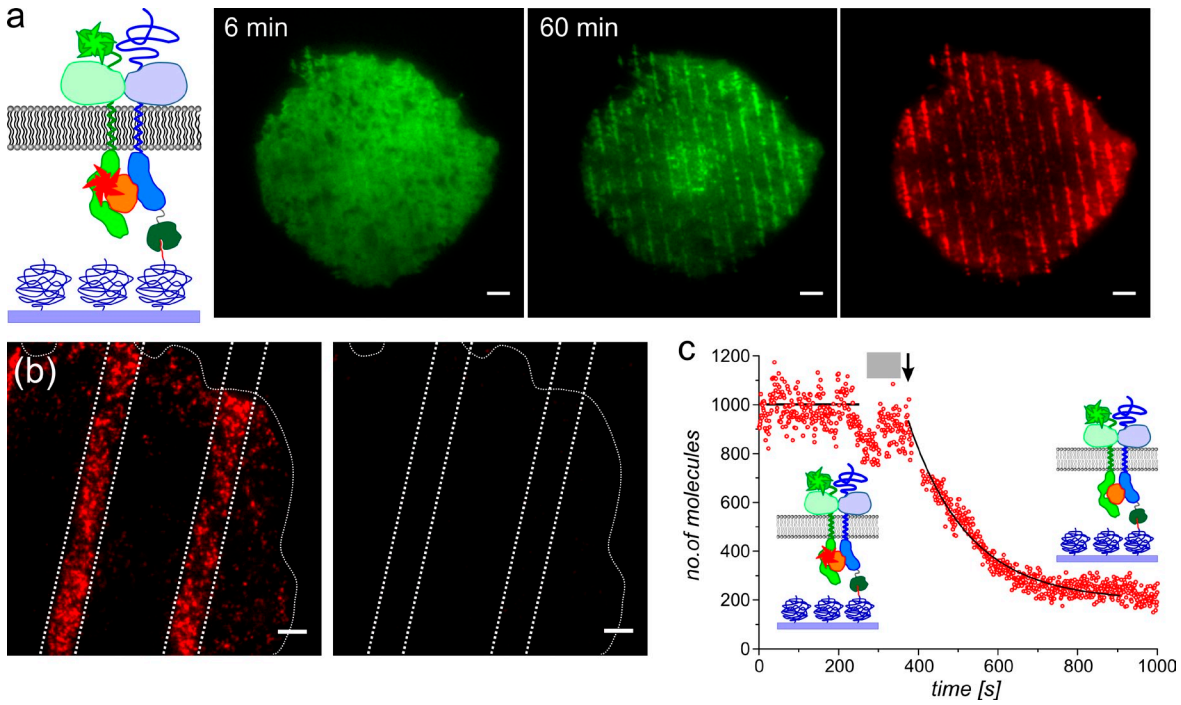

Figure 4. **Reversible IFNα2 binding to both IFNAR1 and IFNAR2.** (a) HaloTag-IFNAR2 expressed in HeLa cells together with IFNAR1-EGFP (green channel) and cultured on a micropatterned support at different times after injection of ^{AT655}IFNα2 (red channel). Bars, 10 µm. (b) Micropatterns after binding of 0.5 nM ^{DY647}IFNα2 M148A (left) and after addition of unlabeled IFNα2-α8tail-YNS (right). Dotted lines indicate the analyzed line pattern. Bars, 5 µm. (c) Displacement kinetics in micropatterns after addition of unlabeled IFNα2-α8tail-YNS and a monoexponential fit of the curve (from the cell shown in b, representative of three cells analyzed). The time regimen during injection and refocusing is marked by a gray bar.

signals observed for IFNα2, IFNAR1, and IFNAR2 (Fig. 3 c) clearly confirmed ternary complex formation within micropatterns. Thus, IFN-induced dimerization rather than preassembled dimers was clearly established by using receptor patterning. The kinetics of translocation into the micropatterns was obtained (Fig. 3 d), yielding a rate constant of ∼0.1 min^{-1}. This relatively slow complex formation can probably be explained by diffusion-controlled binding, which is a consequence of the pattern geometry.

To probe the stabilization of IFN binding by interacting with both receptor subunits simultaneously, HeLa cells expressing HaloTag-IFNAR2 and IFNAR1 fused to EGFP (IFNAR1-EGFP) were cultured on micropatterned support. Recruitment of IFNAR1-EGFP into micropatterns upon addition of ^{AT655}IFNα2 was observed (Fig. 4 a), confirming ligand-induced receptor assembly and the versatility of the technique. Moreover, strong binding of ^{DY647}IFNα2 M148A was observed (Fig. 4 b), which requires simultaneous interaction with both IFNAR1 and IFNAR2 for high-affinity binding (Gavutis et al., 2005). The significant binding of ^{DY647}IFNα2 M148A qualitatively confirmed an increase in affinity as a result of ternary complex formation. The complex stability was quantitatively probed in terms of ligand dissociation kinetics by addition of unlabeled IFNα2-α8tail-YNS, yielding complete displacement of ^{DY647}IFNα2 M148A (Video 4 and Fig. 4 b). From the fluorescence decay within the micropattern (Fig. 4 c), a dissociation rate constant of 0.006 ± 0.002s^{-1} was obtained, confirming stabilization by a factor of ∼100 compared with the interaction of IFNα2 M148A with IFNAR2 only (see previous section). This stabilization is in line with binding experiments using radiolabeled IFNs, which suggested an increase in binding affinity upon coexpression of IFNAR1 and IFNAR2 versus IFNAR2 only (Cohen et al., 1995). These experiments confirmed intact functionality of micropatterned IFNAR2 to recruit IFNAR1 into a dynamic ternary signaling complex in the plasma membrane of live cells.

Functional association of the JAKs

To explore the capability of this micropatterned ternary complex to activate intracellular signaling, we first probed the interaction of the tyk2 and Jak1 with IFNAR1 and IFNAR2, respectively. To this end, tyk2 fused to monomeric EGFP (tyk2-EGFP) was coexpressed with IFNAR1 fused to an N-terminal HaloTag (HaloTag-IFNAR1) in HeLa cells, which were cultured on a micropatterned support (Fig. 5 a). Micropatterning of tyk2-EGFP was observed, and colocalization with immobilized IFNAR1 was confirmed by using the IFNα2 variant YNS, which binds IFNAR1 with ∼60-fold increased binding affinity compared with the wild type (Fig. 5 b; Kalie et al., 2007). To exclude that the observed intensity distribution was caused by an increased background excitation as a result of changes in the membrane topography within HTL-functionalized zones, control experiments with cells expressing EGFP and HaloTag-IFNAR2 were performed (Fig. S3). No correlation between the EGFP fluorescence intensity and the micropattern was observed under these conditions, confirming specific association of tyk2 to micropatterned IFNAR1. The stability of this complex was quantitatively probed by FRAP. For this purpose, tyk2-EGFP

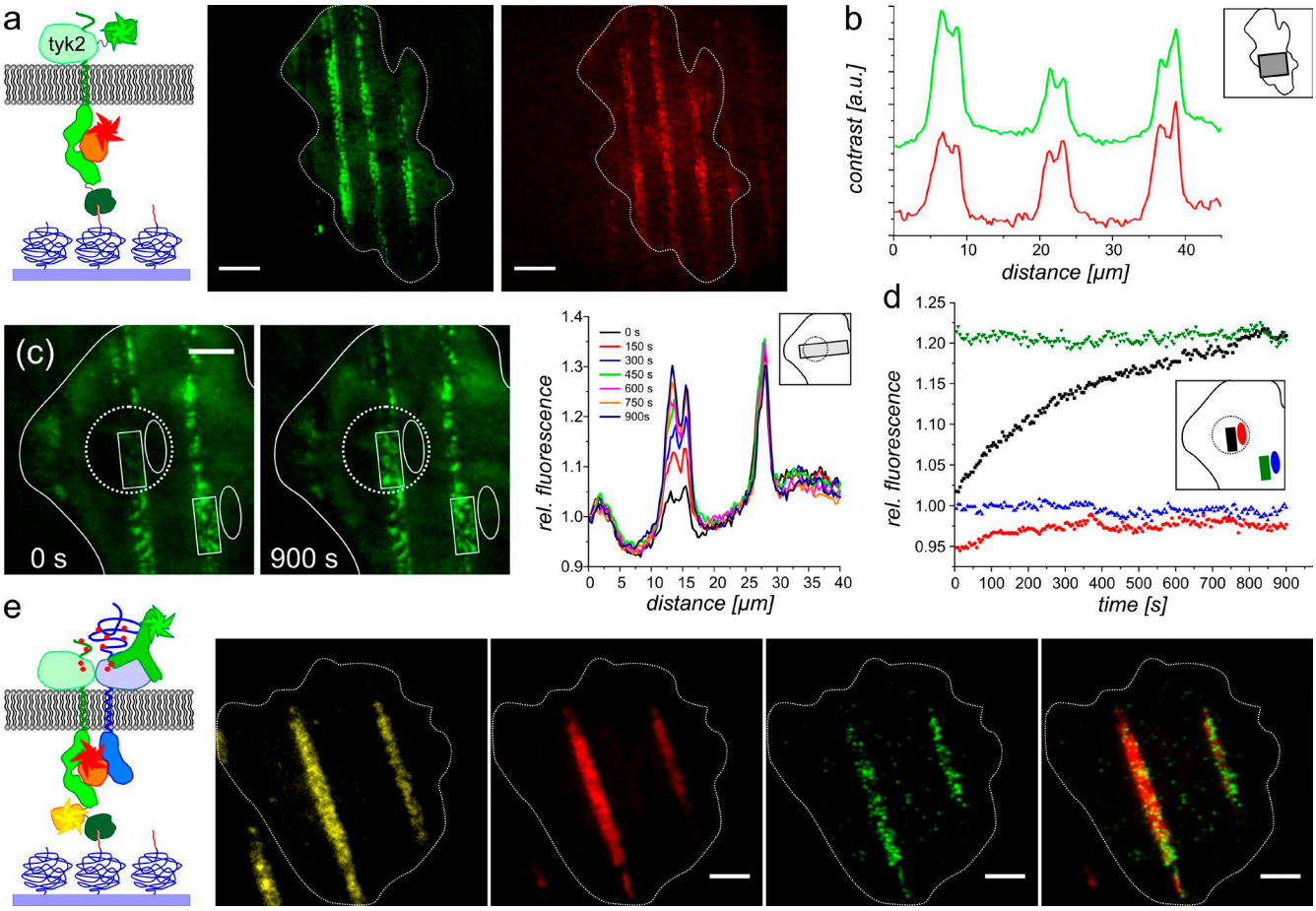

Figure 5. **Recruitment and activation of JAKs.** (a) Binding of tyk2 to micropatterned IFNAR1. HeLa cells cotransfected with HaloTag-IFNAR1 and tyk2-EGFP (green channel) were cultured on a micropatterned support and stained with ^{AT655}IFNα2-YNS (red channel). Cell boundaries are indicated by a dotted line. Bars, 20 µm. (b) Sectional profiles of tyk2 and IFNAR1 fluorescence intensity in the respective channels of a (representative of five cells analyzed). Integrated line profiles were scaled to similar amplitudes and overlaid at an arbitrary ordinate scale. a.u., arbitrary unit. (c) FRAP of tyk2 within the pattern. The bleached area is indicated by a dotted circle. (right) Projected profile across the bleached area as indicated in the inset (representative of four cells analyzed). rel., relative. Bar, 10 µm. (d) FRAP curves obtained in different ROIs within c color coded as indicated in the inset (representative of four cells analyzed). (e) Formation of a functional ternary signaling complex probed by immunostaining of pJak1. HeLa cells were transfected with HaloTag-TagRFP-IFNAR1 (yellow channel) and SNAP-IFNAR2. After addition of ^{AT655}IFNα2 (red channel), cells were fixed and stained via an anti-pJak1 antibody (green channel). Cell boundaries are indicated by a dotted line. Bars, 10 µm.

was bleached within a segment of the micropattern, and the recovery was followed (Video 5 and Fig. 5 c). A comparison of the changes in fluorescence intensity during the FRAP experiment in different regions of the micropattern is shown in Fig. 5 d: Although stable fluorescence signals were obtained both within and outside the micropattern of nonbleached control regions, fluorescence recovery was observed in the bleached area. The minor recovery outside the micropattern could be explained by interaction of tyk2 with other cytokine receptors. However, owing to the small amplitude of this control curve, the exchange kinetics within the micropattern was directly assessed from the recovery curve by fitting a monoexponential function, yielding a rate constant of ∼0.0025 ± 0.001 s^{-1}. As a large excess of tyk2-EGFP is available in the cytosol, this rate constant can be interpreted as the dissociation rate constant of the tyk2–IFNAR1 complex as a rate-limiting step of the exchange.

To explore the formation of an active signaling complex within micropatterns, we probed tyrosine phosphorylation of Jak1, which is critically required for all further signaling cascades. For this purpose, HeLa cells were cotransfected with IFNAR1 fused to the HaloTag and TagRFP (HaloTag-TagRFP-IFNAR1) as well as IFNAR2 fused to the SNAP-tag (SNAP-IFNAR2) and cultured on a micropatterned support. After addition of ^{AT655}IFNα2, cells were fixed and immunostained via an anti-pJak1 antibody. Colocalization of ^{AT655}IFNα2 and HaloTag-TagRFP-IFNAR1 in micropatterns confirmed ternary complex formation. Strikingly, specific binding of the anti-pJak1 antibody into these micropatterns was confirmed (Fig. 5 e), which was not observed in the absence of IFNα2 (Fig. S4). Thus, spatially resolved activation of Jak1 was assayed by this micropatterning method.

Recruitment of STAT proteins

The mechanistic details of STAT recruitment to IFNAR have remained enigmatic. Based on pull-down experiments, STAT2 has been suggested to be constitutively associated with the cytosolic domain of IFNAR2 (Li et al., 1997). This interaction was confirmed by coexpression of HaloTag-IFNAR2 and STAT2 fused to monomeric EGFP (STAT2-EGFP; Fig. 6 a). Colocalization

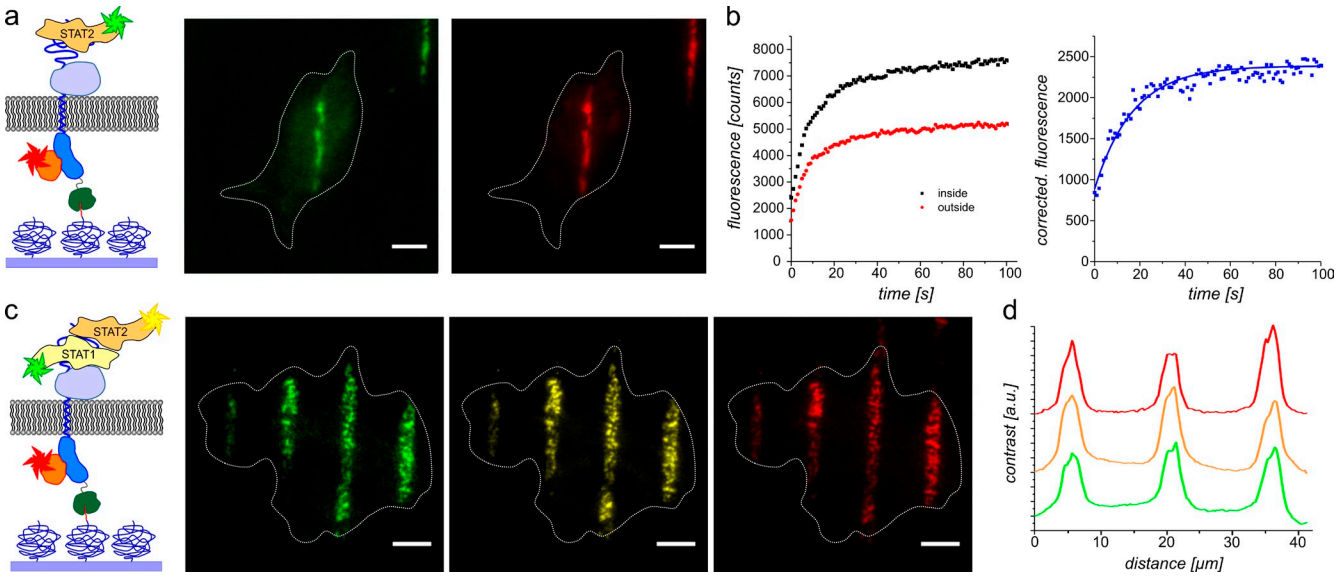

Figure 6. **Recruitment of effector proteins by micropatterned IFNAR.** (a) Constitutive binding of STAT2 to micropatterned Halo-IFNAR2: HeLa cells transfected with HaloTag-IFNAR2 and STAT2-EGFP (green channel). IFNAR2 micropatterning was confirmed by staining with ^{AT655}IFNα2 (red channel). Cell boundaries are indicated by dotted lines. Bars, 10 µm. (b) Dynamics of the STAT2 interaction with micropatterned IFNAR2 probed by FRAP (representative of 10 cells analyzed). (left) FRAP curves inside and outside the IFNAR2 micropattern. (right) Corrected FRAP curve and fit of a monoexponential function. (c) Recruitment of STAT1 to IFNAR2 via STAT2: HeLa cells expressing HaloTag-IFNAR2, STAT1-EGFP (green channel), and STAT2-TagRFP (yellow channel). After image acquisition, IFNAR2 patterning was confirmed by incubation of ^{AT655}IFNα2 (red channel). Cell boundaries are indicated by dotted lines. Bars, 10 µm. (d) Profiles of sectional distribution of fluorescence intensity in each channel in c (representative of six cells analyzed). Integrated line profiles were scaled to a similar amplitude and overlaid at an arbitrary ordinate scale. a.u., arbitrary unit.

of STAT2-EGFP with HaloTag-IFNAR2 in micropatterns was confirmed by subsequent staining IFNAR2 with ^{AT655}IFNα2. The dynamics of STAT2 interaction with micropatterned IFNAR2 in the absence of ligand stimulation was probed by FRAP (Fig. 6 b). Owing to the relatively low contrast observed for STAT2 interaction with IFNAR2 as a result of cytoplasmic STAT2 and the relatively fast recovery in both inside and outside the pattern, this background was subtracted. Thus, a recovery curve specifically representing the exchange kinetics of the IFNAR2–STAT2 complex was obtained, yielding a rate constant of $0.12 \pm 0.05\ s^{-1}$, i.e., ∼50× faster than that observed for JAK binding to the receptor subunits. Upon stimulation with IFNα2, no significant changes in STAT2 interaction with IFNAR2 were observed, yet STAT2 translocation into the nucleus after several minutes confirmed cell viability and functional integrity of the IFN signaling system in micropatterned cells (Fig. S5).

In contrast, only very low colocalization of STAT1-EGFP with micropatterned IFNAR2 was observed (Fig. S5). Furthermore, no constitutive binding of STAT1 to IFNAR1 was detectable, and no significant increase in STAT1 binding upon receptor stimulation was observed (Fig. S5). Because STAT2 has been implicated in the recruitment of STAT1 (Li et al., 1997), we coexpressed STAT1-EGFP and STAT2 fused to tagRFP-T (STAT2-tagRFP) together with HaloTag-IFNAR2 (Fig. 6 c). Strikingly, clear recruitment of both STAT1 and STAT2 to IFNAR2 was observed under these conditions (Fig. 6 d), suggesting that STAT2 supports docking of STAT1 to IFNAR2, probably by STAT1-STAT2 heterodimerization. These results support the observation that STAT2 is required for STAT1 phosphorylation by IFNAR (Improta et al., 1994; Li et al., 1997). To explore changes in STAT recruitment upon formation of active signaling complexes, IFNAR2-deficient cells (U5A) stably expressing SNAP-IFNAR1 and HaloTag-IFNAR2 were transfected with STAT1-EGFP and STAT2-tagRFP and cultured on micropatterned support. Upon addition of IFNα2, a steady increase of the fluorescence intensity at micropatterned IFNAR was observed for both STAT1 and STAT2 for ∼10 min (Fig. 7 a), which was not observed for unstimulated cells. At the same time, the contrast of the micropattern substantially increased. Quantitative analysis of the fluorescence intensity within the micropattern revealed that a maximum intensity was obtained after 5–10 min of receptor stimulation followed by a relatively slow decay (Fig. 7 b). This temporal characteristic of STAT recruitment to IFNAR is in good agreement with the STAT phosphorylation kinetics. Efficient nuclear translocation of STAT1 and STAT2 corroborated the formation of active signaling complexes within micropatterns, assuming that the vast majority of IFNAR2 at the plasma membrane was captured to the surface. These results suggest that additional docking sites for STAT docking may be created by IFNAR phosphorylation, thus enhancing binding of STAT1 and STAT2.

Role of the negative feedback regulator USP18

USP18 has been shown to be an important negative feedback regulator of IFN signaling (Malakhova et al., 2006), which moreover plays a key role in differential IFN signaling (François-Newton et al., 2011, 2012). Because USP18 was shown to bind to IFNAR2 (Malakhova et al., 2006) and has been proposed to affect receptor assembly (Francois-Newton et al., 2011), we here applied the novel features of cell micropatterning for exploring its role in modulating protein interactions involved in the

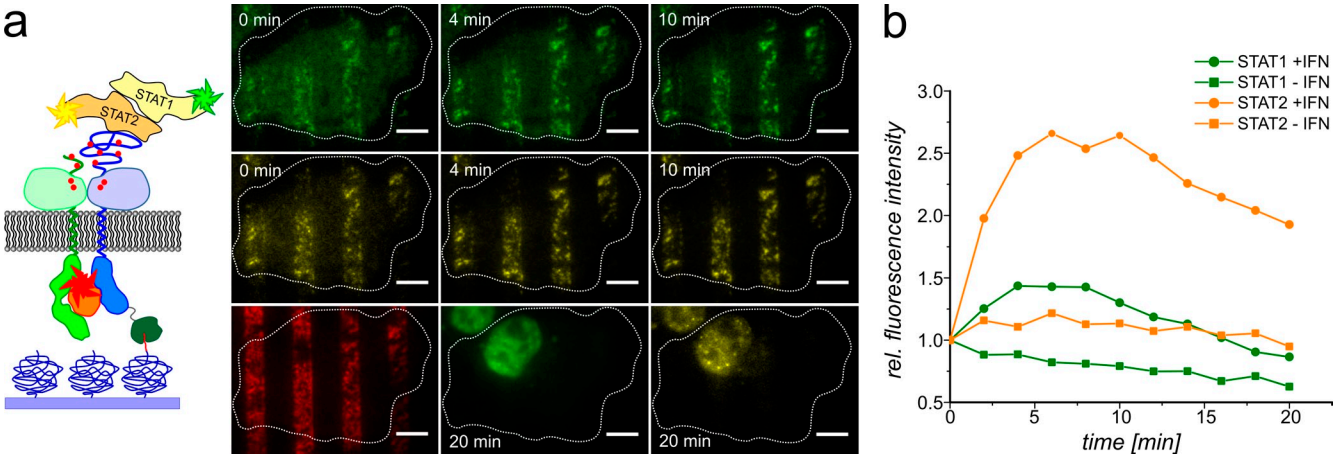

Figure 7. **STAT activation at micropatterned signaling complexes.** (a) U5A cells stably expressing SNAP-IFNAR1 and HaloTag-IFNAR and transiently transfected with STAT1-EGFP (green channel) and STAT2-tagRFP (yellow channel) imaged after stimulation with ^{AT655}IFNα2 (red channel). (bottom center/right) Nuclear translocation of STAT1 and STAT2 20 min after incubation with IFNα2. Cell boundaries are indicated by dotted lines. Bars, 10 µm. (b) Changes in the fluorescence intensity observed for STAT1 and STAT2 within micropatterns compared for stimulated and nonstimulated cells (mean intensity of five ROIs, representative of three cells analyzed). rel., relative.

assembly of the IFNAR signaling complex. Binding of USP18 fused to mEGFP (EGFP-USP18) to micropatterned IFNAR2 independent on receptor dimerization was confirmed (Fig. 8, a and b). To unravel potential inhibition of IFNAR1 recruitment into the ternary complex by USP18 binding, we devised a competition assay for receptor dimerization (Fig. 8 c). For this purpose, HaloTag-IFNAR1 was cotransfected with IFNAR2 and USP18-EGFP as potentially competing interaction partners. In the absence of IFN, homogeneous distribution of USP18 was observed as expected for its interaction with IFNAR2, but not IFNAR1 (Fig. 8 c). Upon ternary complex formation by addition of IFNα2, translocation of USP18 together with IFNAR2 into micropatterns was clearly discerned (Fig. 8, c and d). These experiments revealed that USP18 does not compete with ternary complex formation but rather may act as an allosteric modulator.

We further tested the role of USP18 in assembly of the signaling complex by probing effector interactions in the presence of USP18. Unexpectedly, we unveiled a modulatory role of USP18 in STAT2 recruitment. Upon coexpression of USP18 and STAT2 with the micropatterned IFNAR2, we observed an increased contrast of STAT2. More detailed analysis of the interaction dynamics of the STAT2–IFNAR2 interaction in the presence of USP18 by FRAP (Fig. 8, e and f) revealed a dissociation rate constant of $0.015 \pm 0.005\ s^{-1}$. Thus, USP18 binding to IFNAR2 stabilizes the constitutive STAT2–IFNAR2 interaction by a factor of ∼8. These observations suggest that USP18 may also play a strong regulatory role in STAT signaling.

Discussion

We have here developed a micropatterned surface architecture as a robust platform for spatial organization of proteins within the plasma membrane. Based on a highly biocompatible PEG polymer brush support, nonspecific interaction with the surface is efficiently minimized. We designed a novel photochemical functionalization approach, which yielded highly orthogonal binary patterning, thus ensuring cell attachment via focal adhesions outside the areas functionalized for capturing membrane proteins. Thus, functional receptor micropatterning with good accessibility to the ligand was achieved, providing the capability to probe ligand interaction down to the single-molecule level with extremely low background of nonspecific binding to the coverslide surface. Notably, capturing via the HaloTag as compared with previous approaches based on antibodies ensures high contrast and long-term stability of substrates as well as more robust and generic application, as no suitable antibody toward the bait protein is required.

Based on these systematically engineered surface properties, the assembly of functional transmembrane signaling complexes within micropatterns was possible, including ligand-induced receptor dimerization and the association as well as the phosphorylation of cytosolic effector proteins. Local enrichment of functional bait proteins in the plasma membrane by micropatterned immobilization allows to unambiguously probe cytosolic interaction partners even in the case of promiscuous interactions, e.g., JAKs and STATs, which bind multiple cytokine receptors, and to discriminate membrane binding from background fluorescence. Moreover, immobilization of the micropatterned bait protein excludes lateral diffusion and therefore enables versatile quantitative assays for protein interaction analysis in the context of an intact plasma membrane within live cells. Thus, FRAP experiments in micropatterns allow for quantitatively probing the stability of transient interactions with high specificity. Based on this approach, we succeeded in addressing several fundamental concepts in cytokine signaling for the IFNAR as a model system: (a) ligand-induced heterodimerization of IFNAR1 and IFNAR2 in contrast to currently debated modes of preassembled subunits (Krause et al., 2013) was clearly demonstrated; (b) relatively stable association of the corresponding Jaks with the cytosolic receptor domains was directly shown; (c) stimulation-independent, transient binding of STAT2 to IFNAR2 and the recruitment of STAT1 via STAT2 could be shown as well as increased STAT recruitment to the activated signaling complex; and (d) the interaction of the negative feedback regulator USP18

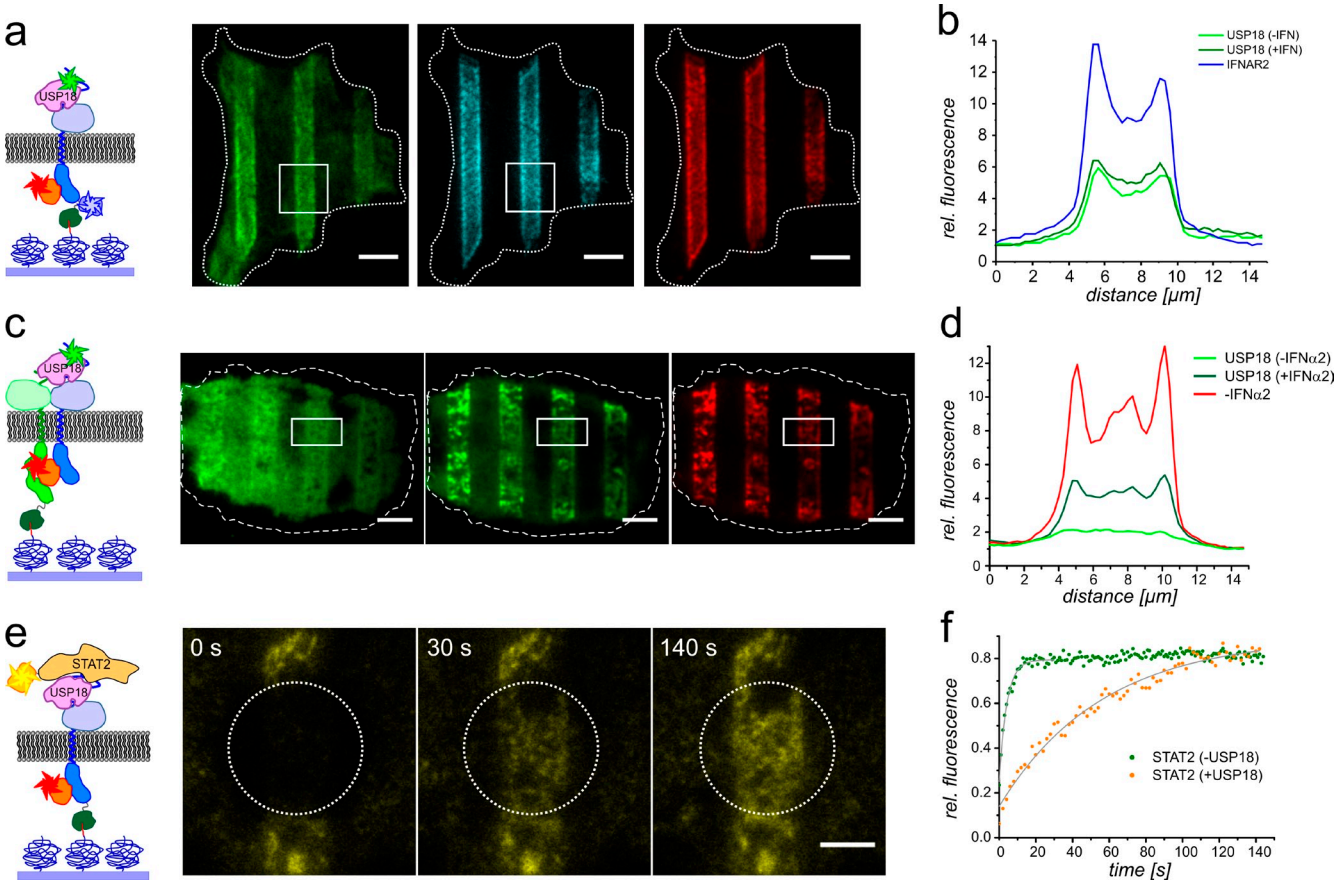

Figure 8. **Role of the negative feedback regulator USP18 for IFNAR dimerization and STAT recruitment.** (a and b) USP18 constitutively binds to IFNAR2: (a) HeLa cells transfected with HaloTag-tagBFP-IFNAR2 (cyan channel) and EGFP-USP18 (green channel) after incubation of ^{AT655}IFNα2 (red channel). Cell boundaries are indicated by dotted lines. The squares indicate the analyzed sectional distribution of fluorescence intensity shown in b. Bars, 10 µm. (b) Contrast of USP18 before and after incubation of ^{AT655}IFNα2 compared with HaloTag-tagBFP-IFNAR2 (representative of three cells analyzed). (c and d) Ternary complex formation and USP18 binding to IFNAR2 are noncompetitive: U5A cells transfected with HaloTag-IFNAR1, SNAP-IFNAR2, and EGFP-USP18 (green channel) before and after addition of IFNα2 (red channel; representative of three cells analyzed). Cell boundaries are indicated by dotted lines. The rectangles indicate the analyzed sectional distribution of fluorescence intensity shown in d. Bars, 10 µm. (d) Intensity pattern in the area indicated in c. (e and f) The stability of constitutive STAT2 binding to IFNAR2 is affected by USP18: (e) STAT2-tagRFP (yellow channel) bound to micropatterned HaloTag-IFNAR2 in cells coexpressing USP18 was bleached with a 405-nm laser in the indicated area (dotted circles), and recovery was monitored. Bars, 5 µm. (f) Comparison of the fluorescence recovery of STAT2 bound to IFNAR2 in the absence and in the presence of ectopic USP18 (representative of 10 cells analyzed in the absence of USP18 and five cells analyzed in the presence of USP18). rel., relative.

with IFNAR2 and a novel role in modulating STAT recruitment could be identified. Thus, we succeeded in acquiring a detailed picture of the dynamics of the entire signaling complex and its negative feedback regulation.

Monitoring homo- and heterodimerization of membrane proteins and the interaction with cytosolic proteins is not only important for cell surface receptors but also for transport machineries and metabolic membrane protein complexes. In this context, cell micropatterning will be particularly valuable for reliably validating and quantifying interactions identified by genome-wide screening techniques (Lam and Stagljar, 2012). However, overexpression of interaction partners is required for optimum contrast, which requires careful interpretation of the biological relevance of experimentally observed interactions. Although we used here a photochemical micropatterning approach, the concept is well compatible with microcontact printing, which allows higher sample throughput. By combination with immunofluorescence labeling, identification of interaction partners and posttranslational modifications will be possible as demonstrated here for Jak1 phosphorylation. Thus, a broad application for unraveling protein–protein interactions at the plasma membrane can be envisaged for this generic, tag-based approach.

Materials and methods

Proteins and plasmids

IFNα2 and mutants fused to an N-terminal ybbR-tag (Yin et al., 2005; IFNα2, IFNα2-YNS, IFNα2 M148A, IFNα2 M148A-NLYY, and IFNα2-α8tail-YNS) for site-specific posttranslational labeling were cloned by insertion of an oligonucleotide linker coding for the ybbR peptide (DSLEFIASKLA) into the NdeI restriction site upstream of the corresponding genes in the plasmid pT7T3-U18cis (Piehler and Schreiber, 1999). Proteins were expressed in *Escherichia coli* (TG1 strain) at 37°C. After solubilization of inclusion bodies and refolding by dilution with 0.8 M arginine (Kalie et al., 2007), the proteins were purified by anion exchange chromatography (HiTrap Q; GE Healthcare) as described previously for wild-type IFNα2 (Piehler et al., 2000b). The proteins were labeled with ATTO 655 (ATTO-TEC) or DY-647 (Dyomics) conjugated to coenzyme A

via enzymatic phosphopantetheinyl transfer and purified by size exclusion chromatography as described previously (Waichman et al., 2010). A degree of labeling >90% was obtained for all IFNα2 proteins as determined by UV/visible spectroscopy. The binding affinities of different mutants are summarized in Table S1. HaloTag-EGFP with a His tag cloned into pET28b was produced in *E. coli* (BL21 strain) at 37°C and purified by immobilized metal ion affinity chromatography followed by size exclusion chromatography as previously described (Liße et al., 2011). The HaloTag-EGFP fusion protein was provided by D. Liße (University of Osnabrück, Osnabrück, Germany). Protein expression in HeLa cells was performed under control of the cytomegalovirus promoter using the pDisplay (Invitrogen) and the pSEMs-Snap-1-26m (Covalys Biosciences) vector backbones. The murine Ig κ-chain leader sequence was used for protein targeting into the plasma membrane. IFNAR1-EGFP was expressed under the control of the SRα promoter using the pMET7 (Takebe et al., 1988) vector backbone. Cloning details of all constructs used in this study are summarized in Table S2.

Synthesis of maleimido-RGD

Maleimido-functionalized RGD synthesis was carried-out using a 1–4-bis(maleimido)butane linker and a short peptide sequence, Ac-CGRGDS-COOH. 6.5 mg Ac-CGRGDS-COOH (Coring System Diagnostix) in 0.5 ml 1-M Hepes buffer, pH 8.0, was mixed with 10 mg 1,4-bis(maleimido)butane in 1 ml DMSO (Sigma-Aldrich) for 1 h at room temperature. The mixture was diluted in water and loaded on a C_{18} reverse-phase HPLC column for purification using a 0–70% acetonitrile gradient in 0.1% trifluoroacetic acid (Sigma-Aldrich)water. Purified maleimide-RGD was lyophilized as a white powder and stored at −20°C. Electrospray ionization mass spectrometry was a mass per charge of 883.1; calculated $[M]^+$ was 883.

Surface modification and photopatterning

Surface silanization, covalent attachment of a thin PEG polymer brush (2,000 g/mol; Rapp Polymere), and further functionalization with maleimide groups were performed as described in detail previously (Piehler et al., 2000a; Waichman et al., 2010). Surface chemistry was performed on standard glass coverslides (1.5 mm) for fluorescence microscopy or on reflectance interference spectroscopy transducers for functional surface characterization (see following section). After surface cleaning in freshly prepared Piranha solution (one part 30% H_2O_2 and two parts concentrated H_2SO_4—caution, highly corrosive), the surface was activated by reaction with pure (3-glycidyloxypropyl) trimethoxysilane (Sigma-Aldrich) for 1 h at 75°C. Thereafter, the surface was reacted with molten diamino-PEG (RAPP Polymere) for 4 h at 75°C and then extensively rinsed with water. Subsequently, 1 M mercaptoethanol in *N,N*-dimethylformamide (Sigma-Aldrich) was incubated for 10 min at room temperature to block the remaining thiol-reactive sites on the surface. For functionalization with maleimide groups, the amine-functionalized surfaces were incubated with a saturated solution of 3-(maleimido)propionic acid *N*-hydroxysuccinimide ester in dry *N,N*-dimethylformamide for 30 min at room temperature. Photolithographic patterning was performed in the presence of 10–20 mM maleimido-RGD in dimethyl sulfoxide by irradiation for 6 min through a photomask using a 75-W Xenon lamp equipped with a 280–400-nm dichroic mirror (Newport Spectra-Physics). Thereafter, the chemically modified slides were carefully washed with DMSO, chloroform, and absolute ethanol and then incubated with 500 µM HaloTag Thiol (O4) Ligand (Promega) for 1 h at room temperature.

Surface binding assays

Label-free monitoring of protein binding to surfaces was performed by reflectance interference spectroscopy using a home-built setup as described previously in detail (Piehler and Schreiber, 2001). Nonpatterned, maleimide-functionalized surfaces (prepared as described in the previous paragraph) were irradiated in the presence of maleimido-biotin for different exposure times. After mounting and equilibrating in Hepes-buffered saline, the amount of immobilized biotin groups was quantified by monitoring binding of 100 nM streptavidin in real time under continuous flow through conditions. For probing binding of HaloTag protein to micropatterned surfaces, 100 nM purified HaloTag-EGFP protein was incubated for 15 min at 37°C followed by three washing steps with medium. Subsequently, EGFP was imaged by confocal laser scanning microscopy (FluoView 1000; Olympus).

Cell culture, binding assays, immunostaining, and fluorescence imaging

HeLa cells were plated in 60-mm cell-culture dishes containing MEM supplemented with 10% fetal calf serum (Biochrom AG), 1% Hepes buffer (PAA Laboratories), and 1% nonessential amino acids (PAA Laboratories) as well as penicillin and streptomycin (PAA Laboratories) to a density of ∼50% confluence and transfected by calcium phosphate precipitation as described earlier (Muster et al., 2010). Cells were plated on micropatterned functionalized coverglass 48 h after transfection and cultured for 15–20 h. For live cell imaging, the medium was exchanged for medium without phenol red. Immunostaining was performed after fixing cells with paraformaldehyde by standard protocols using a pJak-specific polyclonal rabbit antibody (Santa Cruz Biotechnology, Inc.).

Fluorescence imaging was performed using a microscope (Cell^TIRF Xcellence; Olympus) equipped with lasers at 405, 488, 561, and 640 nm as well as a back-illuminated electron-multiplied charge-coupled device camera (C9100-13; Hamamatsu Photonics). A 60× (U Apochromat N 60×/1.45 NA; Olympus) or 150× TIRF objective (U Apochromat N 150×/1.45 NA; Olympus) was used depending on the resolution needed in the respective experiment. To avoid spectral cross-talk, each channel was interrogated separately by using excitation only with the required laser line in combination with the corresponding single-band emission filter. Data acquisition was performed with the acquisition software Xcellence rt version 1.2 (Olympus).

Fluorescence imaging of transmembrane micropatterns was performed at 37°C in an incubation chamber (Olympus). Imaging was performed with a 60× objective and excitation at 405, 488, 561, and at 640 nm with a typical power output of 0.1–1 mW at the objective. For ensemble ligand binding experiments, 10 nM of wild-type or mutant ^{AT655}IFNα2 was added to the medium. Single-molecule ligand binding experiments were performed in the presence of 0.5 nM ^{DY647}IFNα2 M148A-NLYY or ^{DY647}IFNα2 M148A by TIRF imaging as described previously (Waichman et al., 2011). Imaging was performed at 640 nm with a laser power of 2 mW at the objective in the presence of an oxygen scavenger and a redox-active photoprotectant (0.5 mg/ml glucose oxidase [Sigma-Aldrich], 0.04 mg/ml catalase [Roche], 5% wt/vol glucose, 1 µM ascorbic acid, and 1 µM methyl viologen) to minimize photobleaching (Vogelsang et al., 2008). Under these conditions, the bleaching time constant was typically >100 s, thus excluding significant bias by photobleaching. Ligand dissociation kinetics was probed by chasing with 1 µM unlabeled IFNα2-α8tail-YNS, which binds IFNAR with substantially higher affinity (Levin et al., 2011).

Image analysis and image processing were performed using ImageJ (National Institutes of Health). Image processing comprises cropping, scaling, and rotation as well as adjustment of brightness and contrast levels. Localization and residence times of individual IFNα2 molecules were determined from trajectories obtained by the multiple target tracking algorithm (Sergé et al., 2008) as described previously (Waichman et al., 2011). After filtering for immobile trajectories ($D \leq 0.001$ µm^2/s), only trajectories longer than 10 frames were used to minimize erroneous trajectories. Histograms of the frequency of different residence times were fitted by a biexponential decay function to eliminate the contribution of erroneously connected trajectories.

For probing the ligand dissociation kinetics by chasing, 1 µM unlabeled IFNα2 or IFNα2-α8tail-YNS was added, and the pattern was imaged until no further changes were detectable. For the evaluation, all immobile single molecules within the pattern were localized and counted frame by frame. The decay of the number of localized single molecules during the chasing experiments was fitted by a monoexponential decay function. Protein diffusion in the plasma membrane was analyzed by single-molecule tracking as described previously (You et al., 2010).

FRAP experiments

FRAP experiments were performed by using the pinhole in the TIR condenser of the Cell^TIRF Xcellence microscope for bleaching a circular region with a diameter of 18 µm (60× objective) or 8 µm (150× objective) using the 405-nm or the 488-nm laser for photobleaching. For experiments of cells expressing tyk2-EGFP, a 60× objective with an NA of 1.45 (U Apochromat N 60×/1.45 NA; Olympus) was applied for TIR excitation. By using pinhole controls, a circular region with a diameter of 18 µm was selected to cover the pattern and bleached by 488-nm excitation for 25 s with laser power of 11 mW at the objective. Fluorescence recovery was followed by image acquisition with a cycle time of 1 s and a laser power of ∼1 mW at the objective. For FRAP of STAT2-EGFP, a 150× objective with an NA of 1.45 (U Apochromat N 150×/1.45 NA; Olympus) was used for TIR excitation. A circular area with a diameter of 8 µm was bleached by 405-nm excitation for 5 s with a laser power of 7.5 mW followed by acquisition with a cycle time of 1 s by a 1-mW, 488-nm laser excitation.

Fluorescence intensity values were quantified by using ImageJ software. A rectangular region of interest (ROI) within the bleached area of the pattern and a circular ROI within the bleached area but outside the

patterned area were chosen for obtaining intensity values per pixel over time. FRAP curves were obtained by the following equation:

$$f = \frac{\left(F_{ROI_{inside}} - F_{offset}\right) - \left(F_{ROI_{outside}} - F_{offset}\right)}{\left[\frac{\left(F_{ref} - F_{offset}\right)}{\left(F_{ref_0} - F_{offset}\right)}\right]},$$

with $F_{ROI_{inside}}$ and $F_{ROI_{outside}}$ being the fluorescence intensities inside and outside the pattern, respectively, within the bleached spot. F_{ref} is the fluorescence intensity of an unbleached ROI inside the micropattern, and F_{ref_0} is the fluorescence intensity of this ROI before the bleaching experiment. The offset intensity (F_{offset}) was determined from an ROI outside of the cell and was subtracted from all intensity values. The recovery of the fluorescence intensity was fitted by a monoexponential function.

Online supplemental material

Fig. S1 shows the characterization of functional surface micropatterning. Fig. S2 shows that protein micropatterning in cells is specific and correlates with the surface micropattern. Fig. S3 shows negative control experiments confirming negligible effects of protein micropatterning on the actin skeleton, transmembrane protein diffusion, and on cytosolic protein distribution. Fig. S4 shows a negative control demonstrating specificity of Jak1 phosphorylation in micropatterns. Fig. S5 shows constitutive interaction of STAT2 with IFNAR2, no interaction of STAT1 with IFNAR1, and only very minor interaction of STAT1 with IFNAR2 at endogenous STAT2 expression. Table S1 summarizes the binding affinities of IFNα2 mutants and variants applied in the experiments. Table S2 collects details of the plasmids used in this study. Video 1 and Video 2 shows IFNα2 binding to micropatterned IFNAR2 on a single-molecule level and chasing with unlabeled IFNα2, respectively. Video 3 captures IFNAR2 IFNα2-induced partitioning upon ternary complex formation with micropatterned IFNAR1. Video 4 shows ligand displacement form micropatterned ternary complexes. Video 5 captures FRAP of tyk2 bound to micropatterned IFNAR1. Online supplemental material is available at http://www.jcb.org/cgi/content/full/jcb.201406032/DC1.

We thank Gabriele Hikade and Hella Kenneweg for technical support, Domenik Liße (University of Osnabrück) for the HaloTag-EGFP fusion protein as well as technical advice, and Rainer Kurre of the Center for Advanced Light Microscopy Osnabrück for support with fluorescence microscopy. The vector for expression of tyk2 was obtained from Sandra Pellegrini (Institut Pasteur, Paris, France). USP18 fused to EGFP was obtained from Sylvie Urbé (University of Liverpool, Liverpool, England, UK).

This project was supported by funding from the Deutsche Forschungsgemeinschaft (Sonderforschungsbereich 944) and by the European Community's Seventh Framework Programme (FP7/2007–2013) under grant agreement no. 223608 (IFNaction). S. Waichman was supported by a PhD fellowship from the Minerva Foundation.

The authors declare no competing financial interests.

Submitted: 9 June 2014
Accepted: 29 September 2014

References

Arant, R.J., and M.H. Ulbrich. 2014. Deciphering the subunit composition of multimeric proteins by counting photobleaching steps. *ChemPhysChem*. 15:600–605. http://dx.doi.org/10.1002/cphc.201301092

Arrabito, G., S. Reisewitz, L. Dehmelt, P.I. Bastiaens, B. Pignataro, H. Schroeder, and C.M. Niemeyer. 2013. Biochips for cell biology by combined dip-pen nanolithography and DNA-directed protein immobilization. *Small*. 9:4243–4249. http://dx.doi.org/10.1002/smll.201300941

Barrios-Rodiles, M., K.R. Brown, B. Ozdamar, R. Bose, Z. Liu, R.S. Donovan, F. Shinjo, Y. Liu, J. Dembowy, I.W. Taylor, et al. 2005. High-throughput mapping of a dynamic signaling network in mammalian cells. *Science*. 307:1621–1625. http://dx.doi.org/10.1126/science.1105776

Bleicken, S., M. Otsuki, and A.J. Garcia-Saez. 2011. Quantification of protein-protein interactions within membranes by fluorescence correlation spectroscopy. *Curr. Protein Pept. Sci.* 12:691–698. http://dx.doi.org/10.2174/138920311798841744

Brown, R.J., J.J. Adams, R.A. Pelekanos, Y. Wan, W.J. McKinstry, K. Palethorpe, R.M. Seeber, T.A. Monks, K.A. Eidne, M.W. Parker, and M.J. Waters. 2005. Model for growth hormone receptor activation based on subunit rotation within a receptor dimer. *Nat. Struct. Mol. Biol.* 12:814–821. http://dx.doi.org/10.1038/nsmb977

Cohen, B., D. Novick, S. Barak, and M. Rubinstein. 1995. Ligand-induced association of the type I interferon receptor components. *Mol. Cell. Biol.* 15:4208–4214.

Day, R.N., and M.W. Davidson. 2012. Fluorescent proteins for FRET microscopy: monitoring protein interactions in living cells. *BioEssays*. 34:341–350. http://dx.doi.org/10.1002/bies.201100098

François-Newton, V., G. Magno de Freitas Almeida, B. Payelle-Brogard, D. Monneron, L. Pichard-Garcia, J. Piehler, S. Pellegrini, and G. Uzé. 2011. USP18-based negative feedback control is induced by type I and type III interferons and specifically inactivates interferon α response. *PLoS ONE*. 6:e22200. http://dx.doi.org/10.1371/journal.pone.0022200

François-Newton, V., M. Livingstone, B. Payelle-Brogard, G. Uzé, and S. Pellegrini. 2012. USP18 establishes the transcriptional and anti-proliferative interferon α/β differential. *Biochem. J.* 446:509–516. http://dx.doi.org/10.1042/BJ20120541

Gandor, S., S. Reisewitz, M. Venkatachalapathy, G. Arrabito, M. Reibner, H. Schröder, K. Ruf, C.M. Niemeyer, P.I. Bastiaens, and L. Dehmelt. 2013. A protein-interaction array inside a living cell. *Angew. Chem. Int. Ed. Engl.* 52:4790–4794. http://dx.doi.org/10.1002/anie.201209127

Gavutis, M., S. Lata, P. Lamken, P. Müller, and J. Piehler. 2005. Lateral ligand-receptor interactions on membranes probed by simultaneous fluorescence-interference detection. *Biophys. J.* 88:4289–4302. http://dx.doi.org/10.1529/biophysj.104.055855

Grötzinger, J. 2002. Molecular mechanisms of cytokine receptor activation. *Biochim. Biophys. Acta*. 1592:215–223. http://dx.doi.org/10.1016/S0167-4889(02)00316-6

Haan, C., S. Kreis, C. Margue, and I. Behrmann. 2006. Jaks and cytokine receptors—an intimate relationship. *Biochem. Pharmacol.* 72:1538–1546. http://dx.doi.org/10.1016/j.bcp.2006.04.013

Improta, T., C. Schindler, C.M. Horvath, I.M. Kerr, G.R. Stark, and J.E. Darnell Jr. 1994. Transcription factor ISGF-3 formation requires phosphorylated Stat91 protein, but Stat113 protein is phosphorylated independently of Stat91 protein. *Proc. Natl. Acad. Sci. USA*. 91:4776–4780. http://dx.doi.org/10.1073/pnas.91.11.4776

Jaks, E., M. Gavutis, G. Uzé, J. Martal, and J. Piehler. 2007. Differential receptor subunit affinities of type I interferons govern differential signal activation. *J. Mol. Biol.* 366:525–539. http://dx.doi.org/10.1016/j.jmb.2006.11.053

Kalie, E., D.A. Jaitin, R. Abramovich, and G. Schreiber. 2007. An interferon α2 mutant optimized by phage display for IFNAR1 binding confers specifically enhanced antitumor activities. *J. Biol. Chem.* 282:11602–11611. http://dx.doi.org/10.1074/jbc.M610115200

Kim, S.A., K.G. Heinze, and P. Schwille. 2007. Fluorescence correlation spectroscopy in living cells. *Nat. Methods*. 4:963–973. http://dx.doi.org/10.1038/nmeth1104

Krause, C.D., E. Mei, J. Xie, Y. Jia, M.A. Bopp, R.M. Hochstrasser, and S. Pestka. 2002. Seeing the light: preassembly and ligand-induced changes of the interferon gamma receptor complex in cells. *Mol. Cell. Proteomics*. 1:805–815. http://dx.doi.org/10.1074/mcp.M200065-MCP200

Krause, C.D., G. Digioia, L.S. Izotova, J. Xie, Y. Kim, B.J. Schwartz, O.V. Mirochnitchenko, and S. Pestka. 2013. Ligand-independent interaction of the type I interferon receptor complex is necessary to observe its biological activity. *Cytokine*. 64:286–297. http://dx.doi.org/10.1016/j.cyto.2013.06.309

Kubatzky, K.F., W. Ruan, R. Gurezka, J. Cohen, R. Ketteler, S.S. Watowich, D. Neumann, D. Langosch, and U. Klingmüller. 2001. Self assembly of the transmembrane domain promotes signal transduction through the erythropoietin receptor. *Curr. Biol.* 11:110–115. http://dx.doi.org/10.1016/S0960-9822(01)00018-5

Lam, M.H., and I. Stagljar. 2012. Strategies for membrane interaction proteomics: no mass spectrometry required. *Proteomics*. 12:1519–1526. http://dx.doi.org/10.1002/pmic.201100471

Lamken, P., S. Lata, M. Gavutis, and J. Piehler. 2004. Ligand-induced assembling of the type I interferon receptor on supported lipid bilayers. *J. Mol. Biol.* 341:303–318. http://dx.doi.org/10.1016/j.jmb.2004.05.059

Lamken, P., M. Gavutis, I. Peters, J. Van der Heyden, G. Uzé, and J. Piehler. 2005. Functional cartography of the ectodomain of the type I interferon receptor subunit ifnar1. *J. Mol. Biol.* 350:476–488. http://dx.doi.org/10.1016/j.jmb.2005.05.008

Lanzerstorfer, P., D. Borgmann, G. Schütz, S.M. Winkler, O. Höglinger, and J. Weghuber. 2014. Quantification and kinetic analysis of Grb2-EGFR interaction on micro-patterned surfaces for the characterization of EGFR-modulating substances. *PLoS ONE*. 9:e92151.

Lavoie, T.B., E. Kalie, S. Crisafulli-Cabatu, R. Abramovich, G. DiGioia, K. Moolchan, S. Pestka, and G. Schreiber. 2011. Binding and activity of all

human α interferon subtypes. *Cytokine*. 56:282–289. http://dx.doi.org/10.1016/j.cyto.2011.07.019

Levin, D., D. Harari, and G. Schreiber. 2011. Stochastic receptor expression determines cell fate upon interferon treatment. *Mol. Cell. Biol.* 31:3252–3266. http://dx.doi.org/10.1128/MCB.05251-11

Li, X., S. Leung, I.M. Kerr, and G.R. Stark. 1997. Functional subdomains of STAT2 required for preassociation with the α interferon receptor and for signaling. *Mol. Cell. Biol.* 17:2048–2056.

Li, Z., J.J. Strunk, P. Lamken, J. Piehler, and T. Walz. 2008. The EM structure of a type I interferon-receptor complex reveals a novel mechanism for cytokine signaling. *J. Mol. Biol.* 377:715–724. http://dx.doi.org/10.1016/j.jmb.2007.12.005

Liße, D., V. Wilkens, C. You, K. Busch, and J. Piehler. 2011. Selective targeting of fluorescent nanoparticles to proteins inside live cells. *Angew. Chem. Int. Ed. Engl.* 50:9352–9355. http://dx.doi.org/10.1002/anie.201101499

Los, G.V., L.P. Encell, M.G. McDougall, D.D. Hartzell, N. Karassina, C. Zimprich, M.G. Wood, R. Learish, R.F. Ohana, M. Urh, et al. 2008. HaloTag: a novel protein labeling technology for cell imaging and protein analysis. *ACS Chem. Biol.* 3:373–382. http://dx.doi.org/10.1021/cb800025k

Malakhova, O.A., K.I. Kim, J.K. Luo, W. Zou, K.G. Kumar, S.Y. Fuchs, K. Shuai, and D.E. Zhang. 2006. UBP43 is a novel regulator of interferon signaling independent of its ISG15 isopeptidase activity. *EMBO J.* 25:2358–2367. http://dx.doi.org/10.1038/sj.emboj.7601149

Muster, B., W. Kohl, I. Wittig, V. Strecker, F. Joos, W. Haase, J. Bereiter-Hahn, and K. Busch. 2010. Respiratory chain complexes in dynamic mitochondria display a patchy distribution in life cells. *PLoS ONE*. 5:e11910. http://dx.doi.org/10.1371/journal.pone.0011910

Padilla-Parra, S., and M. Tramier. 2012. FRET microscopy in the living cell: different approaches, strengths and weaknesses. *BioEssays*. 34:369–376. http://dx.doi.org/10.1002/bies.201100086

Pang, X., and H.X. Zhou. 2012. A common model for cytokine receptor activation: combined scissor-like rotation and self-rotation of receptor dimer induced by class I cytokine. *PLOS Comput. Biol.* 8:e1002427. http://dx.doi.org/10.1371/journal.pcbi.1002427

Piehler, J., and G. Schreiber. 1999. Biophysical analysis of the interaction of human ifnar2 expressed in *E. coli* with IFNα2. *J. Mol. Biol.* 289:57–67. http://dx.doi.org/10.1006/jmbi.1999.2726

Piehler, J., and G. Schreiber. 2001. Fast transient cytokine-receptor interactions monitored in real time by reflectometric interference spectroscopy. *Anal. Biochem.* 289:173–186. http://dx.doi.org/10.1006/abio.2000.4920

Piehler, J., A. Brecht, R. Valiokas, B. Liedberg, and G. Gauglitz. 2000a. A high-density poly(ethylene glycol) polymer brush for immobilization on glass-type surfaces. *Biosens. Bioelectron.* 15:473–481. http://dx.doi.org/10.1016/S0956-5663(00)00104-4

Piehler, J., L.C. Roisman, and G. Schreiber. 2000b. New structural and functional aspects of the type I interferon-receptor interaction revealed by comprehensive mutational analysis of the binding interface. *J. Biol. Chem.* 275:40425–40433. http://dx.doi.org/10.1074/jbc.M006854200

Prejean, C., and O.R. Colamonici. 2000. Role of the cytoplasmic domains of the type I interferon receptor subunits in signaling. *Semin. Cancer Biol.* 10:83–92. http://dx.doi.org/10.1006/scbi.2000.0311

Remy, I., I.A. Wilson, and S.W. Michnick. 1999. Erythropoietin receptor activation by a ligand-induced conformation change. *Science*. 283:990–993. http://dx.doi.org/10.1126/science.283.5404.990

Ries, J., and P. Schwille. 2012. Fluorescence correlation spectroscopy. *BioEssays*. 34:361–368. http://dx.doi.org/10.1002/bies.201100111

Roisman, L.C., D.A. Jaitin, D.P. Baker, and G. Schreiber. 2005. Mutational analysis of the IFNAR1 binding site on IFNα2 reveals the architecture of a weak ligand-receptor binding-site. *J. Mol. Biol.* 353:271–281. http://dx.doi.org/10.1016/j.jmb.2005.08.042

Salaita, K., P.M. Nair, R.S. Petit, R.M. Neve, D. Das, J.W. Gray, and J.T. Groves. 2010. Restriction of receptor movement alters cellular response: physical force sensing by EphA2. *Science*. 327:1380–1385. http://dx.doi.org/10.1126/science.1181729

Schmitt, H.-M., A. Brecht, J. Piehler, and G. Gauglitz. 1997. An integrated system for optical biomolecular interaction analysis. *Biosens. Bioelectron.* 12:809–816. http://dx.doi.org/10.1016/S0956-5663(97)00046-8

Schwarzenbacher, M., M. Kaltenbrunner, M. Brameshuber, C. Hesch, W. Paster, J. Weghuber, B. Heise, A. Sonnleitner, H. Stockinger, and G.J. Schütz. 2008. Micropatterning for quantitative analysis of protein-protein interactions in living cells. *Nat. Methods*. 5:1053–1060. http://dx.doi.org/10.1038/nmeth.1268

Sergé, A., N. Bertaux, H. Rigneault, and D. Marguet. 2008. Dynamic multiple-target tracing to probe spatiotemporal cartography of cell membranes. *Nat. Methods*. 5:687–694. http://dx.doi.org/10.1038/nmeth.1233

Strunk, J.J., I. Gregor, Y. Becker, Z. Li, M. Gavutis, E. Jaks, P. Lamken, T. Walz, J. Enderlein, and J. Piehler. 2008. Ligand binding induces a conformational change in ifnar1 that is propagated to its membrane-proximal domain. *J. Mol. Biol.* 377:725–739. http://dx.doi.org/10.1016/j.jmb.2008.01.017

Sun, Y., N.M. Hays, A. Periasamy, M.W. Davidson, and R.N. Day. 2012. Monitoring protein interactions in living cells with fluorescence lifetime imaging microscopy. *Methods Enzymol.* 504:371–391. http://dx.doi.org/10.1016/B978-0-12-391857-4.00019-7

Sunzenauer, S., V. Zojer, M. Brameshuber, A. Tröls, J. Weghuber, H. Stockinger, and G.J. Schütz. 2013. Determination of binding curves via protein micropatterning in vitro and in living cells. *Cytometry A*. 83:847–854. http://dx.doi.org/10.1002/cyto.a.22225

Suter, B., S. Kittanakom, and I. Stagljar. 2008. Two-hybrid technologies in proteomics research. *Curr. Opin. Biotechnol.* 19:316–323. http://dx.doi.org/10.1016/j.copbio.2008.06.005

Takebe, Y., M. Seiki, J. Fujisawa, P. Hoy, K. Yokota, K. Arai, M. Yoshida, and N. Arai. 1988. SR α promoter: an efficient and versatile mammalian cDNA expression system composed of the simian virus 40 early promoter and the R-U5 segment of human T-cell leukemia virus type 1 long terminal repeat. *Mol. Cell. Biol.* 8:466–472.

Thomas, C., I. Moraga, D. Levin, P.O. Krutzik, Y. Podoplelova, A. Trejo, C. Lee, G. Yarden, S.E. Vleck, J.S. Glenn, et al. 2011. Structural linkage between ligand discrimination and receptor activation by type I interferons. *Cell*. 146:621–632. http://dx.doi.org/10.1016/j.cell.2011.06.048

Torres, A.J., L. Vasudevan, D. Holowka, and B.A. Baird. 2008a. Focal adhesion proteins connect IgE receptors to the cytoskeleton as revealed by micropatterned ligand arrays. *Proc. Natl. Acad. Sci. USA*. 105:17238–17244. http://dx.doi.org/10.1073/pnas.0802138105

Torres, A.J., M. Wu, D. Holowka, and B. Baird. 2008b. Nanobiotechnology and cell biology: micro- and nanofabricated surfaces to investigate receptor-mediated signaling. *Annu Rev Biophys*. 37:265–288. http://dx.doi.org/10.1146/annurev.biophys.36.040306.132651

Uzé, G., G. Schreiber, J. Piehler, and S. Pellegrini. 2007. The receptor of the type I interferon family. *Curr. Top. Microbiol. Immunol.* 316:71–95.

Vermeulen, M., N.C. Hubner, and M. Mann. 2008. High confidence determination of specific protein-protein interactions using quantitative mass spectrometry. *Curr. Opin. Biotechnol.* 19:331–337. http://dx.doi.org/10.1016/j.copbio.2008.06.001

Vogelsang, J., R. Kasper, C. Steinhauer, B. Person, M. Heilemann, M. Sauer, and P. Tinnefeld. 2008. A reducing and oxidizing system minimizes photobleaching and blinking of fluorescent dyes. *Angew. Chem. Int. Ed. Engl.* 47:5465–5469. http://dx.doi.org/10.1002/anie.200801518

Waichman, S., M. Bhagawati, Y. Podoplelova, A. Reichel, A. Brunk, D. Paterok, and J. Piehler. 2010. Functional immobilization and patterning of proteins by an enzymatic transfer reaction. *Anal. Chem.* 82:1478–1485. http://dx.doi.org/10.1021/ac902608a

Waichman, S., C. You, O. Beutel, M. Bhagawati, and J. Piehler. 2011. Maleimide photolithography for single-molecule protein-protein interaction analysis in micropatterns. *Anal. Chem.* 83:501–508. http://dx.doi.org/10.1021/ac1021453

Waichman, S., F. Roder, C.P. Richter, O. Birkholz, and J. Piehler. 2013. Diffusion and interaction dynamics of individual membrane protein complexes confined in micropatterned polymer-supported membranes. *Small*. 9:570–577. http://dx.doi.org/10.1002/smll.201201530

Xu, Q., W.C. Lin, R.S. Petit, and J.T. Groves. 2011. EphA2 receptor activation by monomeric Ephrin-A1 on supported membranes. *Biophys. J.* 101:2731–2739. http://dx.doi.org/10.1016/j.bpj.2011.10.039

Yamada, M., I. Takase, and N. Koutou. 1968. Photopolymerization of maleimide and its N-substituted derivatives. *J. Polym. Sci. Pol. Lett*. 6:883–888. http://dx.doi.org/10.1002/pol.1968.110061211

Yin, J., P.D. Straight, S.M. McLoughlin, Z. Zhou, A.J. Lin, D.E. Golan, N.L. Kelleher, R. Kolter, and C.T. Walsh. 2005. Genetically encoded short peptide tag for versatile protein labeling by Sfp phosphopantetheinyl transferase. *Proc. Natl. Acad. Sci. USA*. 102:15815–15820. http://dx.doi.org/10.1073/pnas.0507705102

You, C., S. Wilmes, O. Beutel, S. Löchte, Y. Podoplelowa, F. Roder, C. Richter, T. Seine, D. Schaible, G. Uzé, et al. 2010. Self-controlled monofunctionalization of quantum dots for multiplexed protein tracking in live cells. *Angew. Chem. Int. Ed. Engl.* 49:4108–4112. http://dx.doi.org/10.1002/anie.200907032